Shells, Anti-Shells and Modes in Nuclear Fission

F. Gönnenwein

University of Tübingen, Germany

INTRODUCTION

A tour d`horizon to phenomena in fission is proposed where fragment properties play a decisive role. Beyond Liquid Drop the most relevant property of fragments in this context are besides pairing above all nuclear shell effects. Shell effects influence on mass, stability and deformability. In most cases shell effects are discussed as stabilizing nuclei compared to the Liquid Drop formula. But very often it is forgotten that shell effects can in contrast have a destabilizing effect. To help avoid mistakes it is suggested to distinguish between shell and anti-shell effects. Fragment shells lead to fission modes with characteristic properties as to fragment mass, charge, kinetic energy and angular distributions. A particular issue is where in the course of fission the modes are formed. The discussion covers the range of fissioning nuclei of pre-actinides and actinides. Fission and Quasi-Fission of Superheavy Elements requires a detailed discussion beyond the scope of the present survey.

SHELLS AND ANTI-SHELLS

In a simple version of the Liquid Drop Model (LDM) nuclear masses M are parameterized by

$$M(A,Z) = a_V A + a_s A^{2/3} + a_C Z^2/A^{1/3} + a_I (N-Z)^2/A - \delta(A) \quad (1)$$

with the individual contributions called Volume, Surface, Coulomb, Symmetry and Pairing term. The LDM parameters are found from a fit to experimental masses. The LDM masses M_{LDM} are hence averages over experimental masses M_{exp}. For any specific nucleus there is a mass difference δW defined as

$$\delta W = M_{exp} - M_{LDM} \quad (2)$$

A first comprehensive evaluation of δW was published in 1966 [1]. The result in Fig. 1 shows the dependence of δW as a function of neutron number N. Evidently the LDM averages with δW = 0 over N ranges where nuclei are stronger or lesser bound and hence more or less stable. Periodic fluctuations of nuclear stability are explained by the shell model of nuclear structure. In a central nuclear potential the density of energy levels to be occupied is fluctuating: regions of nucleon numbers with higher and lower density of levels compared to average are alternating.

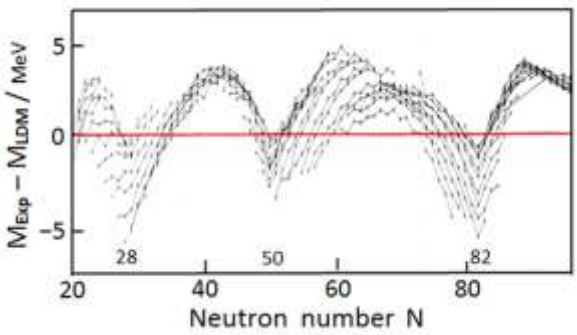

Fig. 1: Shell correction δW vs. neutron number.

For nuclei with bunched occupation levels the total energy (mass) is lower and the stability higher than in the LDM. In these cases the shell correction is negative (δW < 0) and the nuclei are addressed as shell stabilized. In Fig. 1 the magic shell neutron numbers N = 28, 50 and 82 of particularly stable nuclei are catching the eye. However, for nuclei with lower than average

occupied states the total energy (mass) is higher and stability lower than in the LDM. In these cases the shell correction δW is positive (δW > 0).Very often it is forgotten that the shell correction is nearly as often negative or positive. To avoid mistakes, in the following we will speak about a shell effect for δW < 0 and about an anti-shell effect for δW > 0.

For discussing fission phenomena the shell corrections for fission fragments near scission are relevant taking into account deformations and deformation dependent shell effects. Shell corrections for fission fragments are presented in Fig. 2 for four standard fission reactions, either neutron induced or spontaneous[2].A very important feature of shell corrections is their

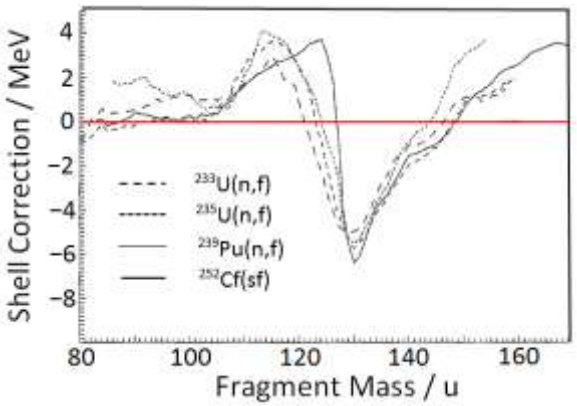

Fig.2: Shell correction δW for fission fragments.

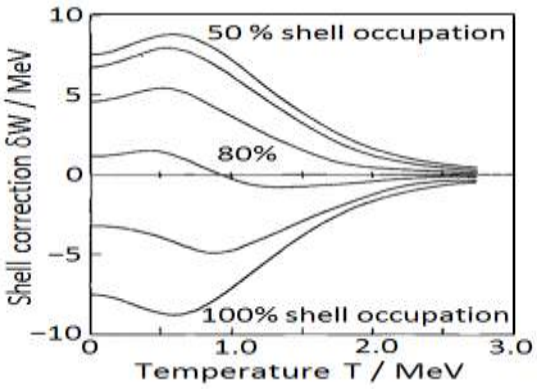

Fig. 3: Shell corrections vanish at T ≈ 2 MeV.

vanishing when the excitation energy of nuclei is raised. This is shown in Fig. 3 for both, shell and anti-shell effects [3].

It has further to be noted that shell effects not only affect mass corrections δW but also the stiffness of nuclei. To deform a nucleus from the spherical shape to an elongated shape, e.g. a spheroid, energy has to be provided which is stored as deformation energy E_{def}. The deformation energy is parameterized as

$$E_{def} = \alpha(D - R_o)^2 \qquad (3)$$

with α the stiffness parameter, R_o the radius of the spherical nucleus getting deformed and D the major semi-axis of the spheroid, nuclear volume being kept constant. For the LDM α is calculated as $\alpha = 2.86 - 0.0630(Z^2/A)$ MeV/fm² by Bohr and Wheeler [4]. An experimental result is given in Fig. 4 [5]. The stiffness parameter $C_2 \sim \alpha$ relative to the LDM value $C_{2\,LDM}$ is plotted as a function of the shell correction δW. The stiffness C_2 was found in experiments on Coulomb excitation of collective vibrations in (e-e) nuclei. The results demonstrate that compared to LDM not unexpectedly shell nuclei with δW< 0 are stiffer and anti-shell nuclei with δW > 0 are softer. There is thus a clear correlation between shell correction and stiffness.

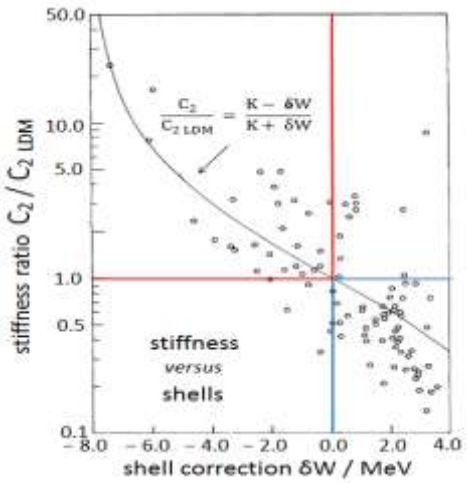

Fig. 4: Stiffness *vs* shell correction.

There is thus a clear correlation between shell correction and stiffness. This correlation is the key for understanding kinetic energies and neutron emission from fragments as a function of their mass. Most conveniently the impact of shells is discussed in a static Scission Point Model (SPM).

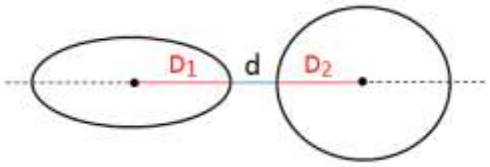

Fig. 5: Geometry of SPM.

In the model the scission configuration is visualized by two more or less elongated spheroidal fragments aligned on a common axis, the fission axis. The tip distance d between the two fragments is held fixed with d = 3 – 4 fm. The potential energies involved at scission are the Coulomb energy V_{Coul} of repulsion between fragments and the energies of deformation V_{Def} of the two fragments. Neglecting the nuclear interaction the total potential energy is

$$V = V_{Coul} + V_{Def} = Z_1Z_2/(D_1+D_2+d) + \alpha_1(D_1-R_{01})^2 + \alpha_2(D_2-R_{01})^2$$

The energy disposable in fission is the Q-value of the reaction. The Q-value goes to

$$Q = TKE + TXE = (V_{Coul} + E_{Kpre}) + (V_{Def} + E_{int}^*) \quad (4)$$

The energy not bound as potential energy is F = Q – V. The quantity F is sometimes misleadingly called "free" energy because it is free to feed the pre-scission kinetic energy E_{KPRE} and the intrinsic excitation energy at scission E_{int}^*. A quasi-static scission configuration is attained for a minimum in the potential and a maximum in the free energy. It is found from $\partial F / \partial D_1 = 0$ and $\partial F / \partial D_2 = 0$. These conditions lead to the relation

$$E_{Def1} / E_{Def2} = \alpha_2 / \alpha_1. \quad (5)$$

This equation tells that in the combination of a soft fragment 1 (α_1 small) and a stiff fragment 2 (α_2 large) the soft fragment gets the larger share of the total deformation energy.

As shown in the following even the present very elementary discussion of shells and anti-shells in nuclei allows appreciating some surprising features in the total kinetic energy and the neutron emission from fragments.

EXAMPLES OF SHELL-ANTISHELL EFFECTS IN THE TOTAL KINETIC ENERGY OF FRAGMENTS

In low energy fission of actinides the dip in the total kinetic energy of fragments (TKE) near mass symmetry is spectacular. A classic example for $^{235}U(n_{th},f)$ is recalled in Fig. 6 [6]. The low TKE near symmetry and the large TKE at the onset of asymmetric fission is understood in terms of shell and anti-shell effects. For near-symmetric fission two fragments with A ≈ 120 and hence δW > 0 appear. They are particularly soft (see Fig.4) entailing elongated scission configurations. The Coulomb energy of interaction will therefore be small which means low TKE. Neighboring events with the heavy fragment $A_H \approx 132$ have δW < 0 while for the complementary fragments with $A_L \approx 100$ the shell correction is δW = 0. Due to the

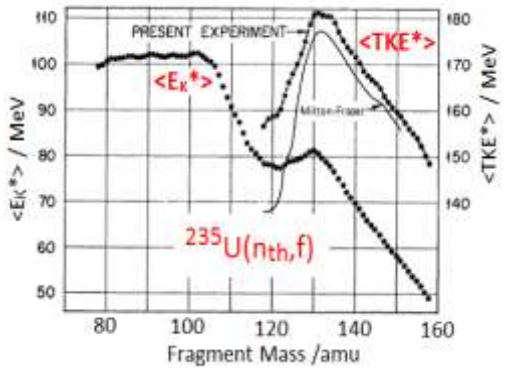

Fig.6: Kinetic energy *vs* FF mass.

strong shell effect for A ≈132 the stiffness against deformation is large (see Fig. 4) and the nucleus remains virtually undeformed at scission. In the resulting compact scission configuration the Coulomb repulsion and hence the TKE will be large.

It is interesting to follow the evolution of TKE for increasing excitation energy of the fissioning nucleus. The example chosen is again for the reaction ^{235}U(n,f) with incoming neutron energies between thermal and 6 MeV. In Fig. 7 it is seen that TKE averaged over all fragment masses decreases at higher excitation energy [2]. However, in the more detailed Fig.8 the difference between TKE at E_n = 6 MeV and at thermal neutron energies, TKE near

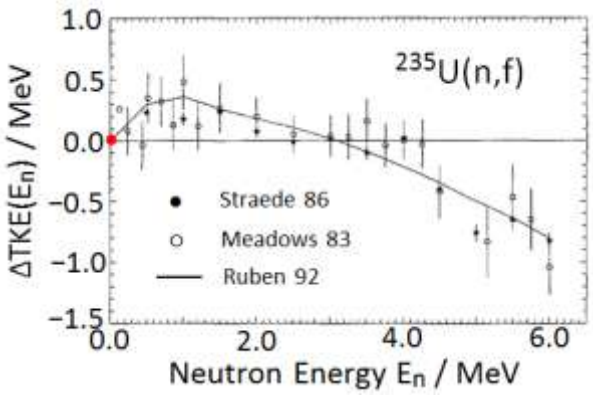

Fig. 7: TKE *vs* incoming neutron energy in ^{235}U(n,f).

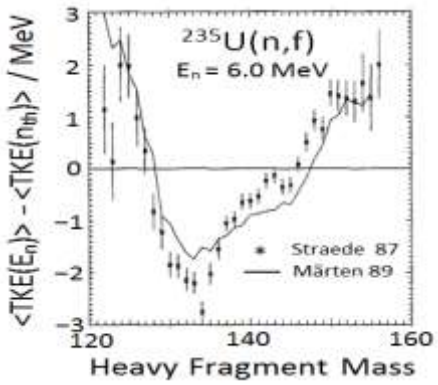

Fig. 8: TKE at E_n = 6 MeV–TKE at th. energy.

A = 120 and for A > 145 increase while only for A = 132–145 TKE decreases [2]. This precisely corresponds to the fading of anti-shell and shell effects with nuclei becoming stiffer or softer, respectively.

SHELLS AND ANTI-SHELLS IN NEUTRON MULTIPLICITY

The famous sawtooth of neutron emission number, the neutron multiplicity, as a function of fragment mass is one of the best memorized features of nuclear fission. It is on display in Fig. 9 for ^{252}Cf(sf) [7]. Over the years it has been studied very often and the reaction ^{252}Cf(sf) has become a standard for the calibration of neutron detectors. Comparing the neutron sawtooth *versus* fragment mass with the shell correction *versus* fragment mass, the similarity between the two functions is striking. Evidently the sawtooth ν(A) comes about through a combination of an anti-shell effect for fragment masses near A = 120 and a shell effect for A = 132. The SPM explains the relative deformation energies and hence the available energies for neutron multiplicities.

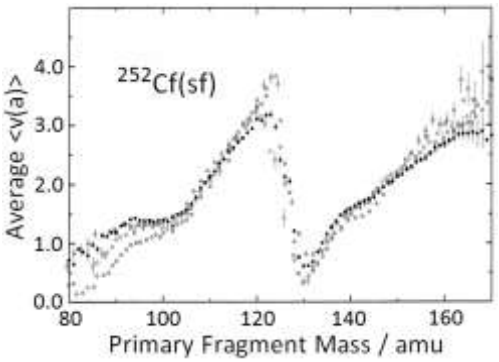

Fig. 9: Sawtooth of neutron multiplicity.

With increasing excitation energy both, shell and anti-shell effects are fading. Shell nuclei become softer and anti-shell nuclei become stiffer. This is reflected as a smoothing of the neutron sawtooth ν(a) in Fig. 10 [8]. With excitation energy increasing the neutron sawtooth disappears completely and multiplicity approaches the expectation from the LDM: ν(A) ~ A. Recall that in the LDM there are no shell nor anti-shell effects.

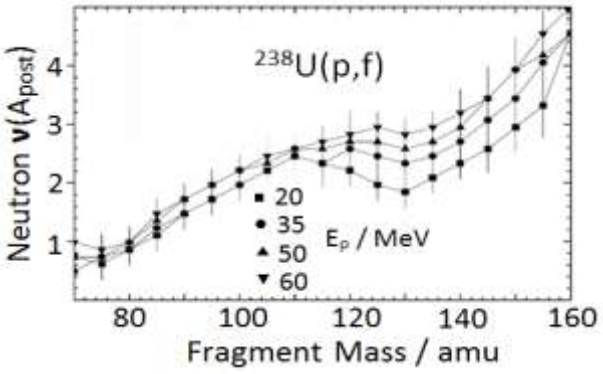

Fig. 10: Neutron multiplicity *vs* fragment mass.

TURKEVICH-NIDAY MODES

Very soon after the discovery of fission it became known that in binary fission of actinides the fragment mass distributions Y(A) are dominantly asymmetric with one heavier and one lighter fragment. There is, however, always also a minor symmetric component. The observation of different asymmetric and symmetric yields and different dependences on excitation energy of yields sparked the suggestion that two different reaction channels are operative. The notion of two different fission MODES, asymmetric and symmetric, was introduced by in 1951 by Turkevich-Niday [9]. An example is shown in Fig. 11 for the reaction ^{235}U(n,f) with incoming neutron energies between thermal and 14 MeV [10].

Insight came with the discovery of shells and anti-shells in nuclei describing microscopically nuclear structure not covered by the LDM. The position of the asymmetric mode is centered at fragments with a spherical shell effect for Z = 50 and N = 82 and a deformed shell effect for N = 88. In symmetric fission near mass A = 120 anti-shell effects prevail as already pointed out in connection with the TKE of fragments. Though there is from experiment a clear correlation between yields and shell effects in the fragments, it requires elaborate Scission Point Models to exploit the correlation and to predict mass distribution Y(A) and kinetic energies of fragments [11,12].

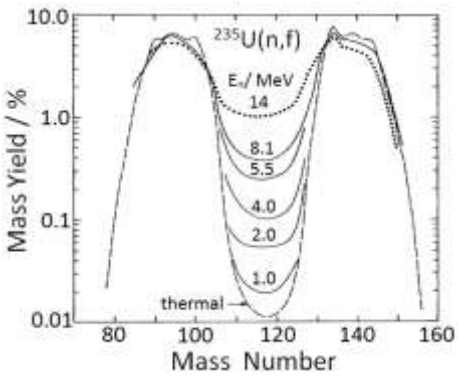

Fig. 11: Mass yields in ^{235}U(n,f).

The difference in mass yields suggests that the barriers having to be overcome in fission are different for the two modes. There has therefore been much work in a variety of theoretical models studying the potential energy surface (PES) between saddle and scission. It is generally accepted that a cut through PES along the minimum path to scission has a double-humped shape as plotted in Fig. 12. Starting at the ground state a first saddle has to be overcome. At this saddle the nucleus is axially asymmetric along the elongation axis but symmetric in mass. In a second minimum of the PES there is a bifurcation between two paths. One path leads to a higher barrier symmetric in mass, while in a second path a lower asymmetric barrier is reached. The evolution of shapes is depicted in Fig. 13 [13]. In this figure it is also indicated that from saddle to scission there is a high ridge between the asymmetric and the symmetric valley. The ridge prevents fission events to spill over the ridge. There is hence a clean separation between the symmetric and asymmetric mode. The separation is confirmed in experiment [14]. Usually it is said that asymmetric fission is

steered by fragment shell effects while symmetric fission is called LDM fission because apparently no structure effects intervene. This is not quite correct since in symmetric fission the fragments have a positive anti-shell correction $\delta W > 0$.

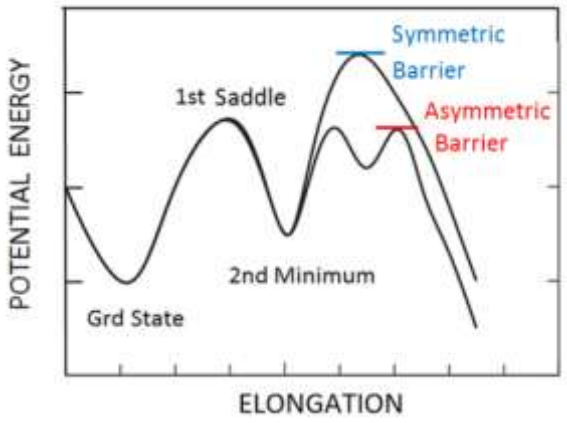

Fig. 12: PES from ground state to scission.

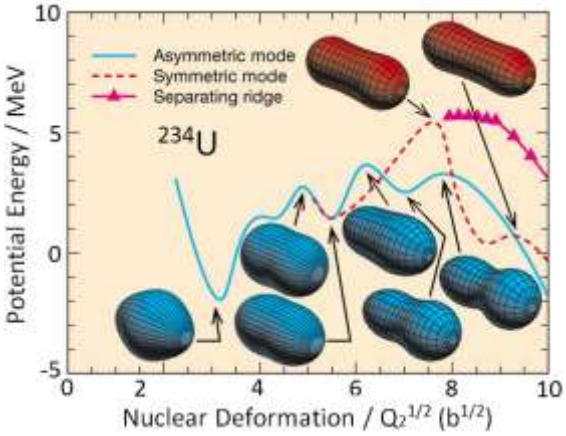

Fig. 13: Nuclear shapes in fission of ^{234}U.

BROSA MODES IN THE ACTINIDES

In fragment mass and energy distributions of asymmetric fission there is a pronounced fine structure. The structure is described by Brosa as a superposition of two modes, "Standard I" and "Standard II". An example for the reaction ^{240}Pu(sf) is provided in Fig. 14 [15]. The modes are ascribed to two different shell effects in heavy fragments. For standard I spherical

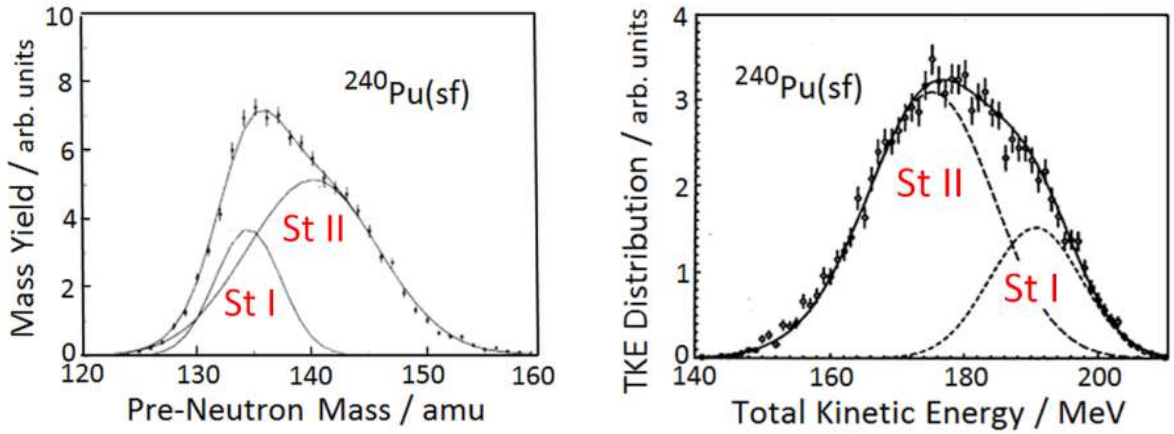

Fig. 14: Brosa modes Standard I and standard II in ^{240}Pu(sf).

shells near Z = 50 and N = 82 are invoked while for Standard II the deformed neutron shell near N = 88 is held to be responsible. The two standard modes are complemented by Brosa by the symmetric Turkevich-Niday mode under the new name "Superlong".

An analysis of mass yield Y(A) and TKE of fragments from ^{235}U(n_{th},f) is presented in Fig. 15 [16]. All three modes are assumed to be parameterized by Gaussians with centers and widths found from fits to experiment. The average heavy mass of the three modes SL, St I and St II are $\langle A_{HF} \rangle$ = 118, 134 and 141 u, respectively. The average total kinetic energy are $\langle TKE \rangle$ = 157, 187 and 167 MeV respectively. The three modes are superposed independently. As

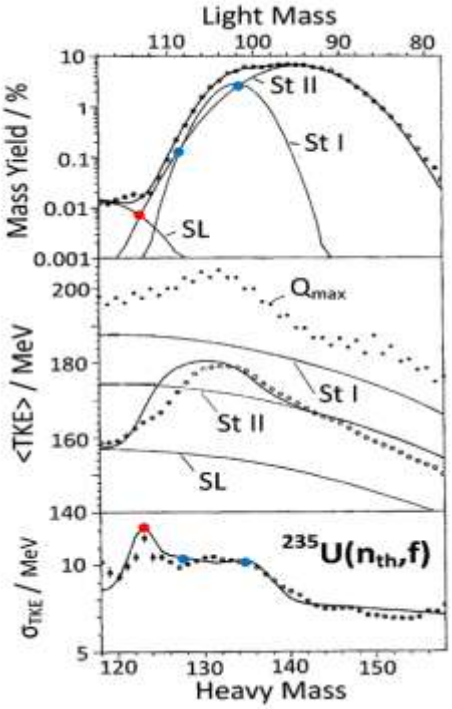

demonstrated in the figure the description by these three modes of mass and TKE is quite good. In particular it should be pointed out that the spike in the variance σ_{TKE} of TKE in the lowest panel of Fig. 15 is located at the mass where the two modes SL and St I overlap. This is a direct proof that these two modes do not mix. Besides the three main modes there is one further mode with very low yield in the tail of the mass distribution Y(A).

Fig. 15: Mode deconvolution of ^{236}U*.

FISSION OF NUCLEI LIGHTER THAN ACTINIDES

By contrast to fission of actinides, in fission of lighter nuclei symmetric fission is dominant. The contribution of asymmetric fission is marginal. An example is given in Fig. 16 for the mass distribution of the fissioning nucleus ^{207}Bi at different excitation energies U at the saddle [17].

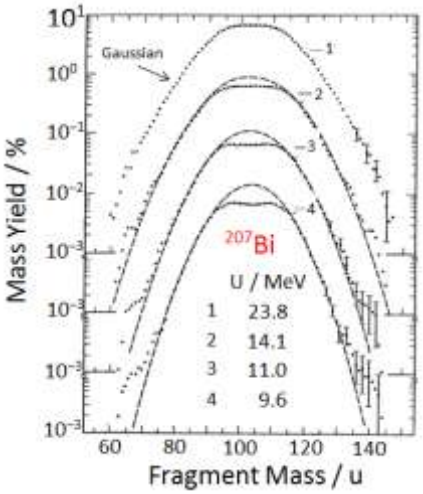

Fig. 16: Mass distribution in the fission of ^{207}Bi.

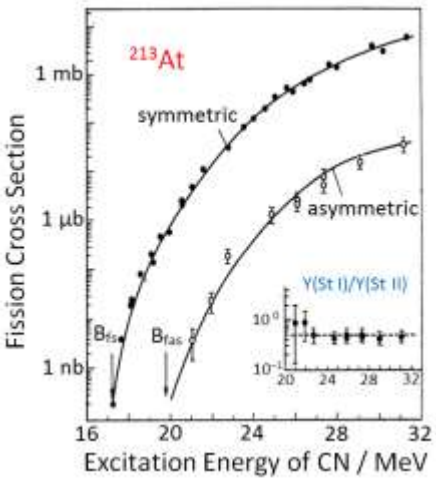

Fig. 17: Fission barriers of the nucleus ^{213}At.

The characteristic features of the mass distributions are reflected in the fission barriers shown for ^{213}At in Fig. 17 [18]. Symmetric fission has the lower barrier just opposite to fission in the actinides (see Fig. 12).

Traditionally symmetric fission is discussed in the framework of the LDM. The shell corrections being possibly present are neglected in a first approximation. It is further taken advantage of the fact that for light nuclei the potential energy drop ΔV between saddle and scission goes to zero: $\Delta V \rightarrow 0$. This means that the scission point coincides with the saddle point. This is the basis for the transition state theory of mass distributions. The LDM approach to the potential energy surface PES is presented in Fig. 18 [19]. The mass dependent "conditional" barrier at the saddle is parameterized as $B_f(A) = B_f(A_{CN}/2) + \frac{1}{2}q_{as}(A - A_{CN}/2)$ in Fig. 18 with q_{as} the rigidity parameter against asymmetric nuclear deformation. According to Bohr-Wheeler the fission rate r(E) is $r(E) \sim \int_0^{E-B_f} \varrho(U)dU$ with $\rho(U) \sim \exp 2(aU)^{1/2}$ the level density at the saddle point. For $U = aT^2$ the mass distribution becomes symmetric: $Y(A) \sim \exp[-(A-A_{CN}/2)^2/2\sigma_A^2]$ where $\sigma_A^2 = T / q_{as}$.

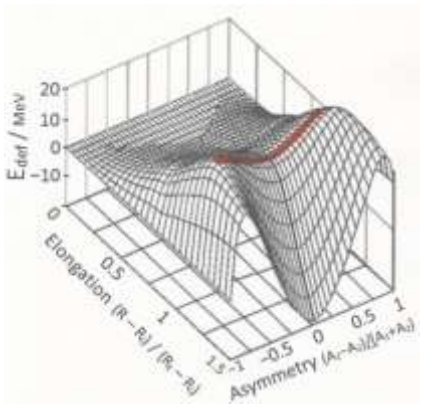

Fig. 18: Conditional LDM barrier.

ITKIS MODES IN LIGHT NUCLEI

Having discussed the interpretation by LDM theory why symmetric mass distributions are favored in fission of light nuclei, the asymmetric component in Y(A) should not be lost out of sight. Asymmetric fission becomes visible in the tails of symmetric mass distributions. A zoom of the mass distributions for ^{213}At, ^{210}Po and ^{205}Bi is on display in Fig. 19 [18]. In the

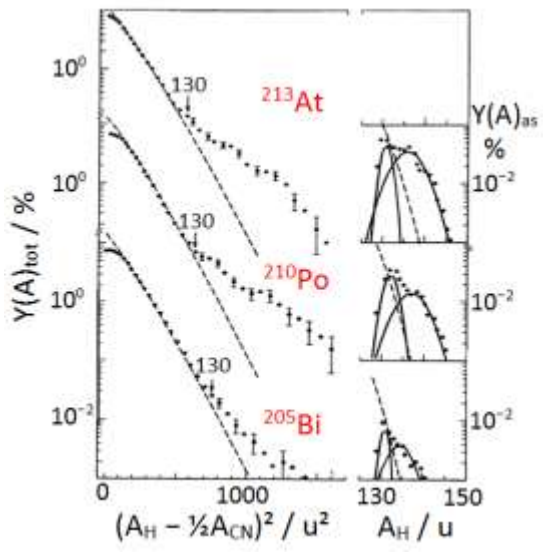

Fig. 19: Asymmetric fission in At to Bi.

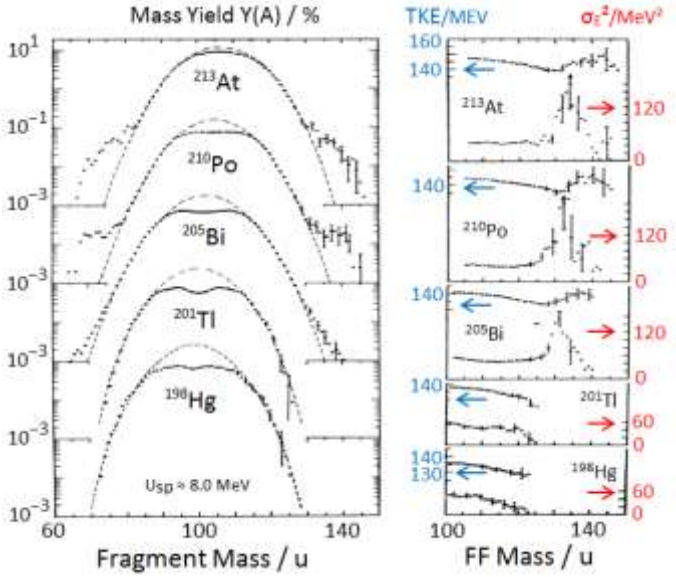

Fig. 20: Survey of mass and energy data for At to Hg.

wings of the distribution a clear deviation from a symmetric Gaussian shows up. Remarkably, like in the actinides, also for light fissioning nuclei the asymmetric mass distribution exhibits a fine structure. The distribution is decomposed into a first Gaussian centered at the heavy

fragment mass $<A_H>$ ≈ 132 u and a second Gaussian at $<A_H>$ ≈ 139 u. These "Itkis" modes are hence identical to the Brosa modes in the actinides.
In the survey of Fig. 20 [20] TKE and variance data are given to the right. As in the actinides in Fig. 15 the variance of TKE has a spike when symmetric and asymmetric modes overlap. A further feature best seen in the TKE data is the disappearance of asymmetric fission for masses of the fissioning nucleus below A ≈ 200 u. Arguments have been given that the high TKE required by asymmetric modes is no longer available from the smaller Q-values of fission reactions for nuclei with $A_H < 200$ u.

At symmetry with fragment mass $A = A_{CN}/2$ the two fragments have neutron numbers close to N = 60. At these neutron numbers there is a pronounced anti-shell effect δW > 0. This gives rise to a bump in the conditional barrier and in consequence to a dent in the yield Y(A). The dent is observed in fission of nuclei from ^{312}At down to ^{198}Hg in Fig. 19. In Fig. 16 the dent in fission of ^{207}Bi is present at low excitation but vanishes at higher excitation for δW→ 0.

ANGULAR DISTRIBUTIONSOF FRAGMENTS

Fission prone nuclei near the saddle point are conveniently approximated by spheroids. Their wave functions are those of symmetric tops. The good quantum numbers are the total angular momentum **J** and the projections of **J** onto both, a space fixed axis M and the symmetry axis of the spheroids K. The symmetry axis becomes the fission axis at later stages of the process. The good quantum numbers from saddle to scission are **J** and M. A. Bohr has postulated that also K is a good quantum number [21]. There is no experimental evidence in conflict with this postulate. In Fig. 21 the different quantities are visualized.

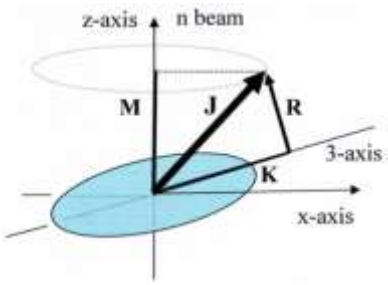

Fig. 21: Angular momenta at saddle.

At scission the fission fragments are ejected along the fission axis. The angular distributions of fragments hence follow the orientation of the fission axis in space.

The distribution is

$$W^J_{MK}(\theta) \sim |D^J_{MK}|^2 \qquad (6)$$

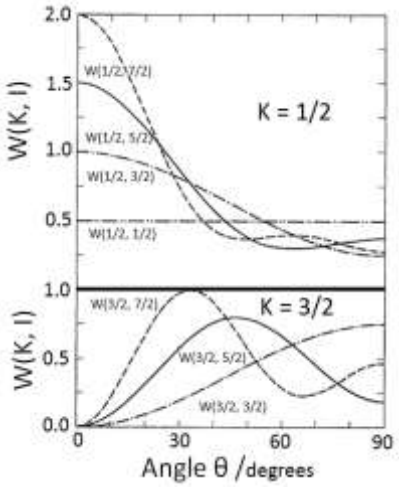

Fig. 22: Angular distributions.

with θ = ∢(n,FF) and D^J_{MK} the wave function of symmetric tops [23]. Focusing on the special case of neutron induced fission of e-e targets one has to consider the target spin **I** = 0, the neutron spin s = ½, the channel spin S = I + **s** = ½, the total angular momentum **J** = **S** + **l**, with **l** the orbital angular momentum imparted to the nucleus by neutron impact and finally M the projection of **J**on the spaced fixed axis (the neutron beam) with M = ± ½ taking into account **l** ⊥ beam axis.
As illustrated in Fig. 22 [22], the angular distributions of all J rotational levels of the K-band carry the same basic characteristic. They are governed by the K quantum numbers. For K = ½ fission fragments are preferentially

ejected at θ = 0° in forward and backward direction relative to the neutron beam. For K = 3/2, 5/2… fragments are emitted by contrast sideways with no emission at all at θ = 0°.

According to A. Bohr not only J but also K stays constant from saddle to scission. The quantum numbers (J,K) of the transition states therefore determine the angular distributions of fragments. For the two Turkevich-Niday modes, symmetric and asymmetric fission, the barriers are different (see Fig. 12). Therefore also the (J,K) quantum numbers of transition states and hence angular distributions differ.

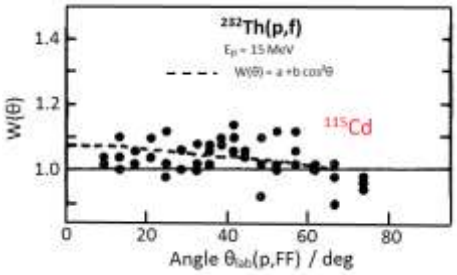

Fig. 23a: W(θ) symm. fission. From [23].

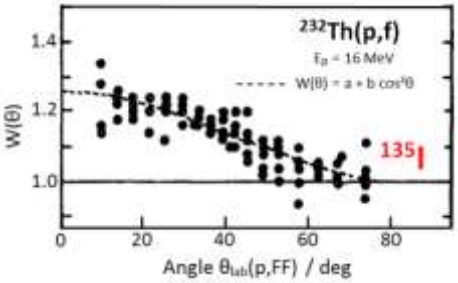

Fig. 23b: W(θ) asymm. fission. From [23].

ANGULAR DISTRIBUTIONS IN BIMODAL ASYMMETRIC FISSION (Brosa Modes)

Example: ^{234}U(n,f)

ABOVE-BARRIER FISSION

According to the A. Bohr postulate the (J,K) quantum numbers of the transition states at the barrier remain the same all over the PES down to scission. Hence the asymmetric Brosa modes St I and St II carry the same (J,K) signature and the angular distributions are identical for the two modes. There is no mass or TKE dependence for $W^J_{MK}(\theta)$ in above-barrier fission as shown in Fig. 25 [24].

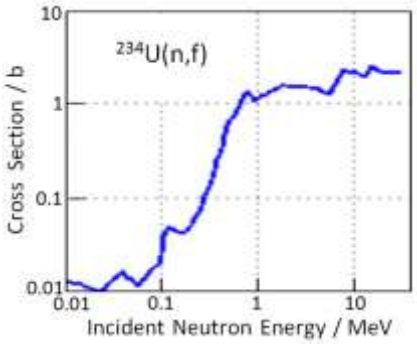

Fig. 24: Fission cross section ^{234}U(n,f).

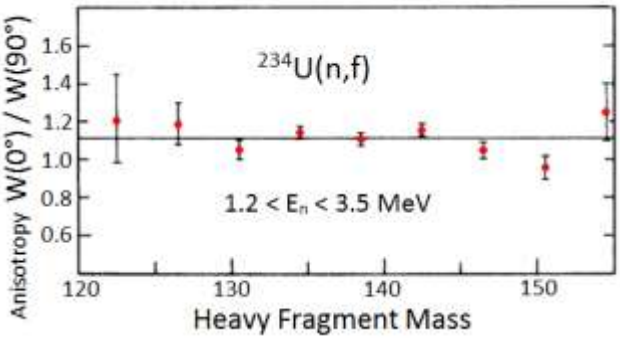

Fig. 25: Above barrier W(0°)/W(90°) ≠ f(A).

SUB-BARRIER FISSION

Sub-barrier fission has been mostly studied near tunnel resonances in (n,f) reactions with (e,e)-targets. For ^{234}U(n,f) mass and energy distributions of fragments were measured at emission angles θ = 0° and 90° *vs* incident neutron energy [25] . Both distributions were observed to depend on the angle θ. The differences Δ of average heavy mass $\langle A_H \rangle$ and energy <TKE> at angles θ = 0° and 90° are on display in Fig. 26. Consider e.g. the resonance at E_n = 0.77 MeV. From $\Delta\langle A_H(\theta)\rangle \neq 0$ and $\Delta\langle TKE(\theta)\rangle \neq 0$ it follows that $\langle A_H(0°)\rangle$ is larger than $\langle A_H(90°)\rangle$ and that <TKE(0°)> is smaller than <TKE(90°)>. Taken together it shows that at θ = 0° the yield ratio St II / St I is larger than at θ = 90°. In particular the mass yield

Y(A) depends on the angle θ and vice versa the angular distribution W(θ) depends on fragment mass A.

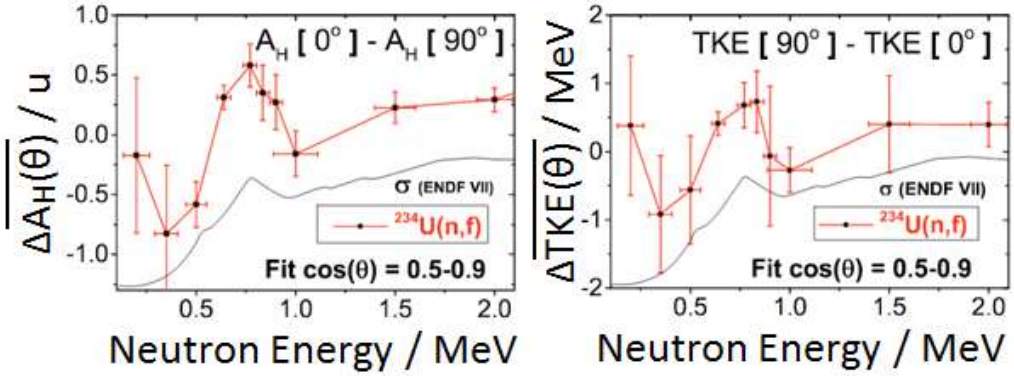

Fig. 26: Differences Δ of $<A_H(\theta)>$ and $<TKE(\theta)>$ between θ = 0° and 90° vs neutron.

A more detailed insight is provided in an experiment where fragment energies TKE are reported separately for the emission angles θ = 0° and 90°. This is shown in Fig. 27 [26]. Take again the resonance at E_n = 0.77 MeV for discussion. According to Fig. 22 at θ = 0° the K = 1/2 and at θ = 90° the K = 3/2 assignment of the wave function is sensed. Near the peak resonance of yield σ_{fi} the TKE data at θ = 0° exhibit a pronounced minimum while for θ = 90° TKE is barely affected. The minimum in TKE is the signature of an increased yield of the mode St II. The interpretation then is that the peak in the cross section is due to a β-vibration in the second minimum of the PES serving as a tunnel transmission resonance through the barrier. The quantum numbers of the vibration are inferred to be K = 1/2. This quantum number assignment is transferred to the valley of mode St II. It is the strong admixture of the tunnel resonance to the total flux tunneling through the barrier which is responsible for the increased fission yield in the σ_{fi}-resonance.

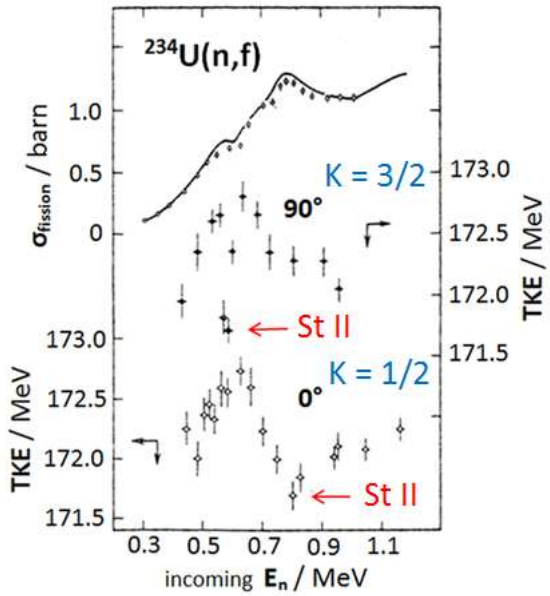

Fig. 27: TKE at θ = 0° and 90°.

In Fig. 27 there are two transmission resonances. As discussed, one at E_n = 0.77 MeV and one at lower neutron energy at E_n = 0.55 MeV (this latter resonance is not visible in the logarithmic plot of Fig. 24). At E_n = 0.55 MeV the peak in the yield is associated with a resonance of TKE at the sideways peaking angle θ = 90° sensing K = 3/2. The minimum of TKE in the resonance is pointing to the preferential feeding of mode St II. The tunnel resonance is therefore attributed the quantum number K = 3/2 feeding preferentially the mode St II. The resonant flux through the barrier is boosting the fragment yield at θ = 90°.Note that The selective feeding of mode St II shows up in Fig. 26 as $\Delta<A_H(\theta)> < 0$ or >0 in the resonances.

The above analysis is corroborated by experimental results on the anisotropy defined as the ratio R of count rates R = W(0°)/W(90°) at the two angles θ = 0° and 90°. Results are on display in Fig. 28 [25]. At the lower resonance for E_n = 0.55 MeV the ratio R is R < 1 while at the resonance for E_n = 0.77 MeV the ratio is R > 0. Preferred sideways emission switches thus at 220 keV higher neutron energy to forward-backward emission.

In summary it has to be stressed that the quantum numbers of the β-vibrations behind the tunnel resonances feed Brosa modes selectively.

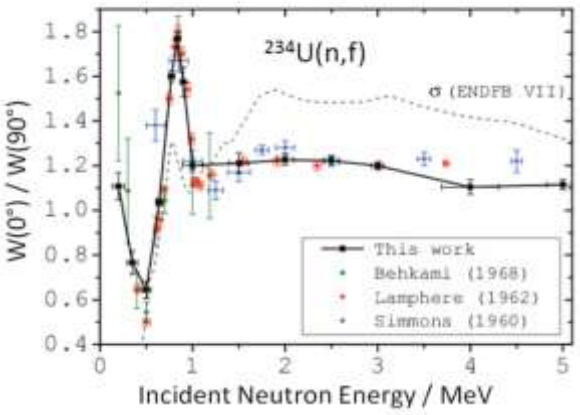

Fig. 28: Anisotropy R = W(0°)/W(90°).

WHERE IN THE COURSE OF FISSION ARE BROSA-ITKIS MODES APPEARING?

The mass and energy dependence of fragment angular distributions in sub-barrier fission may give a key to the issue where in the course of fission the Brosa-Itkis modes are appearing. For fission above the barrier A. Bohr postulates that the (J,K) quantum numbers of the transition states at the barrier impose identical (J,K) assignments in the asymmetric Brosa valleys down to scission. The angular distributions are then identical in the two modes St I and St II, with the corollary that fragment angular distributions are not depending on fragment mass or energy.

By contrast, in sub-barrier fission the angular distributions $W^J_{MK}(\theta)$ depend on the mass and energy of the fission fragments. This is equivalent to state that the modes StI and St II have different (J,K) quantum numbers. Since the total angular momentum J is for given incoming neutron energy a constant of the motion, the K-quantum numbers differ for the two modes. How can this happen?

Model A: The two modes St I and St II have barriers of different height at the saddle. Therefore the (J,K) assignments for the modes are not the same and, like for the symmetric-asymmetric Turkevich-Niday modes, the angular distributions $W^J_{MK}(\theta)$ are different. However, different barriers should also have been observed in above-barrier fission. This has never been found in experiment, nor are there indications from theory. Further the saddle is under-tunneled and not passed. How can saddle transition states influence the tunneling motion?

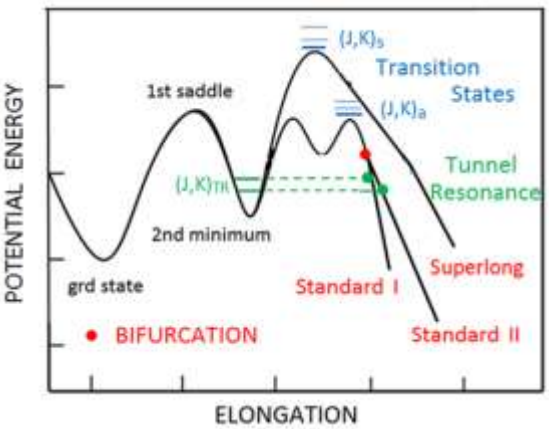

Fig. 29: PES with bifurcation St I ↔ St II.

Model B: Resonances in the sub-barrier fission cross section are traced to vibrational β-resonances in the second minimum of the potential energy surface. From a tunnel resonance with well-defined quantum numbers (J,K) the fissioning system emerges into the PES below the barrier. But this resonance does not feed the modes St I and St II equally. The A. Bohr postulate does not apply. Hence only the angular momentum J is fixed for the process while the K-values will in general not be equal. In consequence the angular distributions for the two

modes are different, $W^J_{MK}(\theta)$ for St I $\neq W^J_{MK}(\theta)$ for St II, and the angular distributions become mass and energy dependent. In this reasoning the asymmetric standard modes come about by a bifurcation on the way from saddle to scission.
This is very similar to the situation in symmetric bimodal fission known in the heavy Fermium isotopes and beyond. Once the symmetric saddle is passed, theory predicts a bifurcation into two symmetric modes [27].

CONCLUSION

In the present survey experimental findings have been brought together where the theoretical concepts of shells, anti-shells and fission modes are catching the eye. Thereby the expression "anti-shell" is introduced for shell corrections $\delta W = M_{exp} - M_{LDM} < 0$ with M the nuclear masses. In these cases nuclei are less stable and softer towards deformation than predicted by the LDM. In current language "shell" effects are usually associated with stable and more rigid nuclei with $\delta W < 0$. The notion of fission "modes" groups together fission fragments with more or less closely related properties as to masses and kinetic energies. They may be found by experiment without introducing the notion of shells. However, they are intimately related to shells and anti-shells. Historically the term fission mode was introduced by Turkevich-Niday for describing phenomenologically the different behaviour of symmetric and asymmetric fission as a function of excitation energy. Later it was shown by theory that symmetric fission is to be understood in terms of the Liquid Drop Model (no shell effects) while asymmetric fission is steered by shell effects in the fragments. For asymmetric fission it was further realized that there is a fine structure in mass and energy distributions. It was discussed by Brosa in the actinides and by Itkis in the pre-actinides to be due to shells in spherical and deformed fragments, respectively. They are nowadays known as Standard I and Standard II modes of bimodal asymmetric fission.
The term "fission mode" was introduced by Turkevich-Niday to address different properties of fragments in symmetric and asymmetric fission. It was later found that the two modes follow different paths at the outer saddle of the Potential Energy Surface. The symmetric saddle is slightly higher than the asymmetric one and, more important, only in asymmetric fission shell effects are relevant. The two valleys in the PES from saddle to scission are separated by a high ridge preventing the mixing of the modes. As to the fine structure in asymmetric fission of actinides and pre-actinides, there is since decades an issue as to where these modes are developed: before, or at, or past the outer saddle of the PES. It is suggested that, surprisingly the study of fragment angular distribution in sub-barrier fission could solve the issue. In particular sub-barrier (n,f) reactions with even-even targets prove to be revealing. In these reactions the standard tunneling process is boosted by resonant tunneling whenever β-vibrations in the second well of the double-humped PES serve as a catalyst for tunneling. This leads to peaks in the fission cross section below the barrier. As to angular distributions, they are steered by the (J,K) quantum numbers at scission. According to A. Bohr the (J,K) of the transition states in above-barrier fission remain valid down to scission. The modes St I and St II hence carry the same (J,K) assignments and the angular distributions are not mode-dependent. However, in the resonances of sub-barrier fission the angular distributions are mode dependent and carry hence different (J,K) signatures. To all evidence, the A. Bohr postulate does not apply to tunnel resonances. Bimodal asymmetric fission then comes about in a bifurcation of the PES past the saddle with the modes in the two PES valleys being fed not equally in sub-barrier resonances.

REFERENCES

[1] W.D. Myers and W.J. Swiatecki, Nucl. Phys. **81**, 1 (966).
[2] A. Ruben and H. Märten, Proc., Dyn. Aspects of Nuclear Fission“, Smolenice, 1992, p 246.
[3] A.S. Jensen and J. Damgaard, Nucl. Phys. A**203**, 578 (1973).
[4] N. Bohr and J.A. Wheeler, Phys. Rev. **56**, 426 (1939).
[5] M. Kildir and N.K. Aras, Phys. Rev. C **25**, 365 (1982).
[6] H.W. Schmitt, J.H. Neiler and F.J. Walter, Phys. Rev. **141**,1146 (1966).
[7] A.S. Vorobyev et al., Int. Sem. “Interactions of Neutrons with Nuclei”, Dubna, 2001, p 276.
[8] V.A. Rubchenya et al., Nucl. Instr. and Meth. A**463**, 653 (2001).
[9] A. Turkevich and J.B. Niday, Phys. Rev. **84**, 52 (1951).
[10] L.E. Glendenin et al., Phys.Rev. C **24**, 2600, (1981).
[11] B.D. Wilkins, E.P. Steinberg and R.R. Chasman, Phys. Rev. C **14**, 1832 (1976).
[12] H. Märten, Conf. “Fiftieth Anniversary of Nuclear Fission”, Leningrad 1989, p.376.
[13] P. Möller, Nature **409**, 788 (2001).
[14] E. Pfeiffer, Z. Physik **240**, 403 (1970).
[15] C. Wagemans and P. Schillebeeckx, Nucl. Phys. A **502**, 287 (1989).
[16] H.-H. Knitter et al., Z. Naturforschung **42**a, 786 (1987).
[17] M.G. Itkis et al., Z. Physik A **320**, 433 (1985).
[18] M.G. Itkis et al., Sov. J. Part. Nucl. **19**, 301 (1988).
[19] D.N. Poenaru, R.A. Gherghescu and W. Greiner, Nucl. Phys. A **747**, 182 (2005).
[20] M.G. Itkis et al., Sov. J. Nucl. Phys. **52**, 601 (1990).
[21] A. Bohr, Proc. “Peaceful Uses of Atomic Energy”, Geneva 1955, Vol. **2,** p. 151.
[22] A.N. Behkami et al., Nucl. Phys. A **118**, 65 (1968).
[23] H. Kudo et al., Phys. Rev. C **25**, 909 (1982).
[24] R. Vandenbosch, J.P. Unik and J.R. Huizenga, Proc. “Phys. Chem. Fission”, IAEA Salzburg, 1965, Vol.**1**, p 547.
[25] A. Al-Adili et al., Phys. Rev. C **93**, 034603 (2016).
[26] A.A. Goverdovski et al., Sov. J. Nucl. Phys. **46**, 396 (1987).
[27] S. Cwiok et al., Nucl. Phys. A **491**, 281 (1989).